APPLIED SCIENCES AND ENGINEERING

Stretchable anisotropic conductive film (S-ACF) for electrical interfacing in high-resolution stretchable circuits

Hyejin Hwang[1†], Minsik Kong[1†], Kyunghwan Kim[2], Doowon Park[1], Sangyeop Lee[3], Soojin Park[3], Ho-Jin Song[2], Unyong Jeong[1]*

In stretchable electronics, high-resolution stretchable interfacing at a mild temperature is considered as a great challenge and has not been achieved yet. This study presents a stretchable anisotropic conductive film (S-ACF) that can electrically connect high-resolution stretchable circuit lines to other electrodes whether they are rigid, flexible, or stretchable. The key concepts of this study are (i) high-resolution (~50 μm) but low–contact resistance (0.2 ohm in 0.25 mm^2) interfacing by periodically embedding conductive microparticles in thermoplastic film, (ii) low-temperature interfacing through the formation of chemical bonds between the S-ACF and the substrates, (iii) economical interfacing by selectively patterning the S-ACF, and (iv) direct interfacing of chips by using the adhesion of the thermoplastic matrix. We integrate light-emitting diodes on the patterned S-ACF and demonstrate stable light operation at large biaxial areal stretching (ε_{xy} = 70%).

INTRODUCTION

Stretchable electronics have been receiving intensive attention for a wide range of potential applications such as stretchable displays (*1*–*4*), electronic skin for robotics (*5*, *6*), and human-machine interfaces such as wearable devices (*7*–*15*) and implantable medical devices (*16*–*18*). With the recent advances in stretchable electrodes and device structures, stretchable electronics are now evolving into high-resolution integrated circuits (*19*–*21*). One of the key technological challenges of high-resolution stretchable devices is stable electrical interfacing between stretchable circuit lines and an external circuit or an operating microchip. In the conventional rigid and flexible electronics, the electrical interfacing is completed through wire bonding (*22*, *23*), via hole (*24*, *25*), and flip-chip bonding (*26*, *27*). However, in the stretchable devices, the large mismatch in elastic modulus between stretchable circuit lines and the rigid or flexible electrodes causes delamination and fracture during repeated stretching cycles (*28*–*32*). Although weak electrical interface is the main cause of device failure in the stretchable electronics and the low-resolution interface is the bottleneck of miniaturized stretchable devices, a small number of the related researches have been carried out for low-resolution interfacing (*11*, *33*–*36*) and high-resolution interfacing has not yet been successful.

Anisotropic conductive film (ACF) is an adhesive surface-mount interconnection that allows only the electrical conduction in the thickness direction. ACF has been widely used primarily for high-density electrical connection in printed circuit boards (PCBs) and device packages (*37*). Most ACFs are thermoplastic or ultraviolet (UV)–curable polymer composites (epoxy, acryl, etc.) with solder balls or conductive microparticles (MPs); hence, they can have good adhesion to substrates, large toughness, high conductivity, and low contact resistance. Several studies on ACF have been conducted for interfacing in flexible devices. Park *et al.* (*38*) have reported an epoxy-based flexible ACF with randomly distributed solder balls (25 to 32 μm in diameter). The random distribution of the solder balls led to a low spatial resolution (~500 μm) that was about 20 times the solder ball size because the aggregated solder balls increased the short-circuit rate of the metal lines to be interfaced. The same group attempted to reduce agglomeration of the conductive MPs by applying a high magnetic field; however, the dispersion rate of the MPs was less than 80% (*39*). Recently, Lee *et al.* (*40*) have proposed selectively dewetted anisotropic patterns through the capillary migration of a metal nanoparticle polymer composite solution, but the random arrangement of the nanoparticles and the poor flexibility are not appropriate for stretchable interconnection.

Most of the current stretchable devices use a stretchable substrate with the rigid islands on which the rigid devices are mounted (*41*). Because the rigid islands are typically designed to experience a small strain (ε < 10%), stretchability of the interface is not a big issue. Ink-jet printing of conductive epoxy ink in the via holes, followed by local heating of the ink at a high temperature (≥180°C), is known to lead to a stable interface (*42*, *43*). However, this rigid island approach with a local heating has a limitation on the achievable spatial resolution. The ultimate direction of interfacing in the stretchable electronics is direct integration of miniaturized devices on the high-resolution stretchable circuit. In addition, in some cases, stretchable circuit lines should be connected to other stretchable circuit lines. The direct integration on a stretchable substrate and the stretchable-stretchable interfacing require large mechanical toughness and the stable adhesion force of the adhesion layer to prevent mechanical failure under a large strain (*29*, *44*, *45*). Toughness of the commercial adhesives that are used in the conventional ACFs are not large enough to endure the large strains ($\varepsilon \geq 50\%$): acryl (1 to 4 MPa/m^2), epoxy (0.5 to 2 MPa/m^2), and silicone rubbers (0.02 to 0.5 MPa/m^2) (*46*). Therefore, a stretchable tough ACF with a strong interfacial adhesion is required. Very recently, a deformable ACF was reported by Lu *et al.* They vertically aligned Ag-coated Ni

[1]Department of Materials Science and Engineering, Pohang University of Science and Technology, 77 Cheongam-Ro, Nam-Gu, Pohang 37673, Republic of Korea. [2]Department of Electrical Engineering, Pohang University of Science and Technology, 77 Cheongam-Ro, Nam-Gu, Pohang 37673, Republic of Korea. [3]Department of Chemistry, Pohang University of Science and Technology, 77 Cheongam-Ro, Nam-Gu, Pohang 37673, Republic of Korea.
*Corresponding author. Email: ujeong@postech.ac.kr
†These authors contributed equally to this work.

MPs (15 μm in diameter) with an average alignment spacing of 50 to 75 μm in a polydimethlysiloxane (PDMS) rubber matrix under magnetic field (*47*). They exhibited mechanical durability of the ACF up to ε = 30%; however, the contact resistance (2.0 ohms per 1 mm^2 contact area) was large and the resolution of reliable interfacing was limited (1 mm) due to the randomness of the alignment. For the use in high-resolution stretchable electronics, ACF requires improved mechanical durability at large tensile strains and precise position control of the conductive fillers. In addition, applying high-pressure or high-temperature thermal annealing in the process of interfacing should be avoided.

In this study, we present a stretchable ACF (S-ACF) in which conductive MPs (20 μm in diameter) are periodically arranged in a thermoplastic block copolymer film. Owing to the precise position registry of the MPs, the S-ACF has a reliable electrical interface with a practically assured fine pitch capability (1200 $μm^2$ for a bump and 52.5 μm for a circuit line) and a low contact resistance (0.19 ohm per 0.25 mm^2). The S-ACF forms strong covalent bonds at the contact interfaces at a mild temperature (80°C); hence, it is applicable to stretchable-stretchable, stretchable-flexible, or stretchable-rigid interfaces. It shows excellent mechanical durability up to ε = 80% without change in conductivity. We demonstrate direct integration of μ-LEDs (light-emitting diodes) on localized S-ACF patterns interfacing stretchable circuit lines. This work is expected to provide new inspiration to the creation of stretchable interfaces and the fabrication of high-resolution stretchable devices.

RESULTS

S-ACF–containing conductive MPs embedded in thermoplastic film

In our previous works, we demonstrated the preparation of high-quality MP monolayers by the mechanical rubbing process (*48*–*50*). In particular, MP separation was possible by putting the MPs in the intaglio patterns such as holes, lines, and squares in elastomer templates (*51*–*55*). Here, the S-ACF was designed to place one MP in each hole made in a thermoplastic block copolymer stencil. We used polystyrene-*block*-poly(ethylene-*ran*-butylene)-*block*-polystyrene-graft-maleic anhydride (SEBS-g-MA) for the stencil and used Au/Ni-coated polystyrene MPs with a diameter (*D*) of 20 μm as the conducting MPs. SEBS-g-MA was selected as the stencil matrix due to its mechanical toughness and chemical reactivity for good adhesion (it will be discussed later). Figure 1A illustrates the manufacturing process of the S-ACF. A slide glass was treated with octadecyl trichlorosilane (OTS) for easy peel-off of the thermoplastic film. A concentrated SEBS-g-MA solution was spin-coated on a PDMS substrate, and the resultant SEBS-g-MA film was transferred to the OTS-treated slide glass. A pillar-patterned stamp made of NOA 61 was placed on the SEBS-g-MA film, pressed vertically under 7 MPa at 180°C for 10 min, and then cooled down naturally in the air. We used the high aspect ratio stamp (≥4) because it made the demolding process easier after the patterning process. With a proper adjustment of the stamp hardness (85D) by UV exposure optimization to the NOA 61 micropillars (see fig. S3 for the optimization conditions), the stamp could be used repeatedly without damage. The depth (t_w) of the template well was controlled by the length of the stamp pillar, and the residual layer thickness (t_r) at the bottom was controlled by the initial film thickness of SEBS-g-MA. t_w was designed to be smaller than *D* to make the MPs exposed to the air. The conductive MPs were rubbed with a piece of PDMS on the template. The MPs were positioned in each well, as shown in the cross-sectional scanning electron microscope (SEM) image (Fig. 1B). Hot pressing was applied on the MP-containing template at 235°C under 57 MPa for 1 hour. For uniform compression, the S-ACF was inserted between two elastomer films, PDMS. The hot pressing is based on the viscoelastic flow of the polymers at the temperature and pressure. We found that the block copolymer chains could make enough fluidity at the temperature at which the block copolymer

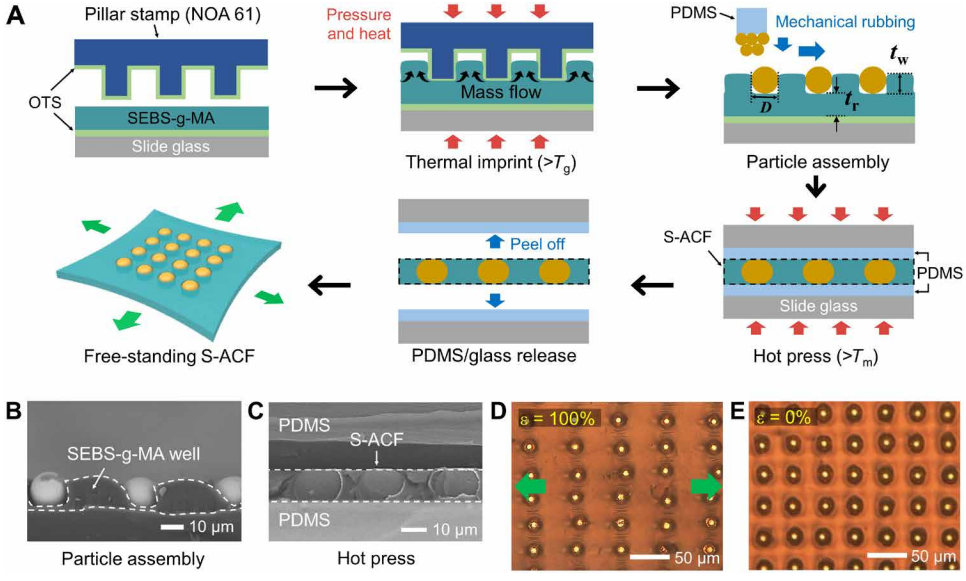

Fig. 1. Fabrication process and microscope images of S-ACF. (**A**) Scheme for the fabrication of the S-ACF. The fabrication process includes microimprinting to create the SEBS-g-MA template, mechanical rubbing of conductive MP powder for particle assembly, hot pressing to MP embedding, and releasing PDMS/glass to obtain the free-standing S-ACF. (**B**) Cross-sectional SEM image taken after the particle assembly in the template. (**C**) Cross-sectional SEM image of the S-ACF after the hot pressing. (**D** and **E**) Optical images of the S-ACF when stretched (ε = 100%) (D) and strain released (ε = 0%) (E).

had the order-to-disorder transition (fig. S1A); thus, the bottom residual layer flew out through the sides. This process made the MPs exposed to the air at both the top and bottom surfaces (fig. S4B). The fabrication of the S-ACF by this hot pressing was highly reproducible. After cooling naturally, the template was peeled off to produce the S-ACF. Details on the fabrication process are described in the Supplementary Materials (see Supplementary Text and figs. S2 and S3).

Figure 1C shows the cross-sectional SEM image of the S-ACF. The metal shell of some MPs was broken when the S-ACF was fractured in liquid nitrogen for SEM specimen preparation. The MPs embedded in the hole were clearly separated from each other. The MPs were flattened at both the top and bottom sides during the hot pressing because the pressing temperature was much higher than the glass transition temperature (~100°C) of the polystyrene core. The flattened metal surface increased the contact area with the electrodes to be integrated; thus, electrical conduction through the S-ACF could be improved. Although the glass transition temperature of the PS core is 100°C, due to the metal shell (Ni/Au) coated on the polymer core (fig. S4A), the conducting MPs were not deformed even at the temperature above 235°C in the absence of mechanical pressure. We did not find any thermal deformation or degradation while driving electronics. After the hot pressing condition, the MPs were exposed at both the top and bottom surfaces (fig. S4B). While the post-thermal pressing at above the order-to-disorder transition temperature was applied, the low viscosity ($<2.3 \times 10^7$ cP) of the polymer matrix resulted in the mass flux to fill the gap in the well between the MPs and the stencil wall. The good adhesion of the MPs with the SEBS-g-MA matrix made the interface stable under a large uniaxial tensile strain (ε = 100%) (fig. S4, C and D). Although the MPs were rigid at room temperature, the composite film was stretchable under repeated stretching, without causing delamination or tearing at the MP-matrix interface (Fig. 1, D and E).

MP periodicity in S-ACF for interfacing high-resolution circuit line

On the one hand, the mass flux during the post-annealing enhanced the adhesion between the MPs and the matrix; on the other hand, a large mass flux in the lateral direction (indicated by the black arrows) moved the MPs (indicated by a violet arrow) and reduced the periodicity (Fig. 2A). Therefore, t_r had to be optimized to achieve both the adhesion and the periodicity of the MPs. Figure 2B shows the MP distribution depending on t_r (1.3, 2.5, 11.3, and 48.1 μm). To clearly visualize the positions of the MPs, Au line patterns (1 mm × 0.2 mm) were sputtered on the PI substrate before the post-annealing. The periodicity of the MPs was kept when $t_r \leq$ 2.5 μm, whereas it disappeared when $t_r \geq$ 11.3 μm. Figure 2C compares the relative change in the number density (N/N_o) of the MPs before (N_o) and after (N) the post-thermal pressing. Optical microscope (OM) images and the raw data are provided in fig. S5 and table S1. When $t_r \leq$ 2.5 μm, N/N_o was close to 1.0 (0.99 at t_r = 1.3 μm and 0.97 at t_r = 2.5 μm), whereas N/N_o decreased to 0.66 at t_r = 11.3 μm. Because a large N/N_o is desired to maximize the electrical conductivity and high-resolution interfacing, the conditions of $t_r \geq$ 11.3 μm were excluded in this study. In addition, Fig. 2C exhibits the dependence of the vertical resistance on t_r. The resistance had a large deviation at t_r = 1.25 μm because the amount of the polymer was not sufficient to fill the void in the well so that the contact between the MP and the electrode was not reliable, causing unstable contact resistance. When t_r = 2.5 μm, the SD was negligible (±0.049) and the resistance was 0.19 ohm/0.25 mm^2, which is much smaller than the reported values (0.3 ohm/6 mm^2) (ECATT 9703; 3 M). We took t_r = 2.5 μm as the optimum condition for the S-ACF. It is notable that the four-point probe measurement was used to measure the vertical resistance of the S-ACF (*39*). The measurement setup is provided in the Supplementary Materials (fig. S6 and table S3).

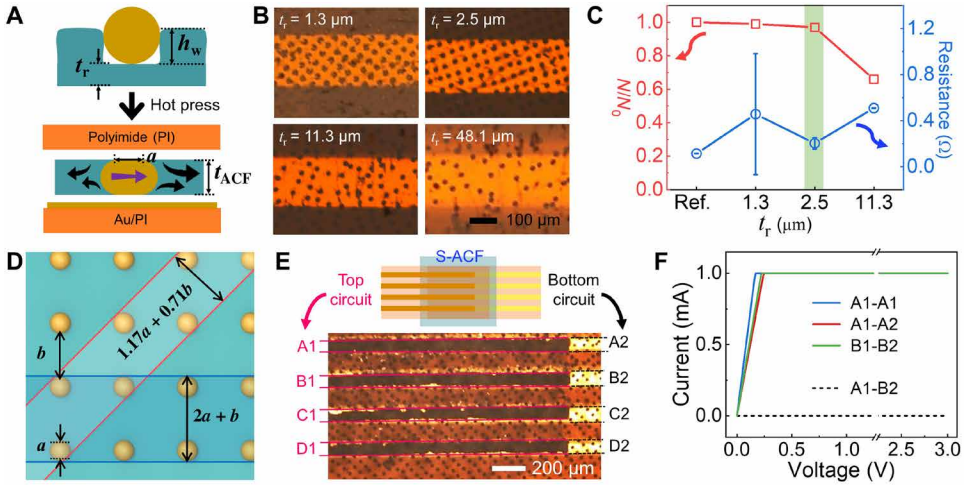

Fig. 2. Optimization of MP periodicity to obtain high electrical performance S-ACF. (**A**) Scheme of the polymer flow during the hot pressing. MP moves (violet arrow) along with the polymer flow (black arrow). Polymer flux to the right direction is presented higher. (**B**) Top-view OM images showing the periodicity of MPs after the hot pressing when the thickness of the residual polymer layer (t_r) was 1.3, 2.5, 11.3, and 48.1 μm. (**C**) Changes in the relative MP density (N/N_0) before (N_0) and after (N) the hot pressing. The interconnection resistance of the S-ACF is measured by the four-point probe. (**D**) Scheme showing the dependence of the MP coverage on the alignment angle with the circuit line direction (red line, blue line). (**E** and **F**) Electrical properties of the optimized S-ACF measured by two-point probe. (E) Top-view scheme and the corresponding OM image of the S-ACF (blue). The S-ACF was sandwiched between top and bottom Au circuit lines. (F) Current-voltage characteristics of a single line (A1-A1) and between the top-bottom connected lines facing each other (A1-A2) and facing aside (A1-B2).

Because the resistance of the S-ACF decreased as the number of MPs in contact increased, the number density of the MPs should be uniform in the entire area of the S-ACF. The requirement can be achieved by the periodic arrangement of the MPs. The minimum contact width (W_{min}) to ensure electrical connection in the S-ACF, which is the spatial resolution of circuit line interfacing, can be calculated under the following assumptions: (i) The MPs are arranged periodically, (ii) the metal circuit line in contact (typically at the millimeter level) is much longer than the MP period, and (iii) all MPs create identical electrical path. Although the ultimate W_{min} can be the same with the diameter of the MP (20 μm), a practical resolution was assured by defining a W_{min} that makes full contact with at least two MPs. Under these assumptions, the minimum interconnection area of the S-ACF was 20 μm × 60 μm. On the other hand, for the circuit line connection, as shown in Fig. 2D, W_{min} is dependent on the alignment angle (θ) between the row of the MPs and the metal line direction, $W_{min} = a + (a + b)\sin\theta$, where "$a$" is the contact length (the area of the MP exposed to the surface) and "b" is the gap distance between the adjacent contact diameter (fig. S7). W_{min} was the largest ($W_{min} = 2a + b$) at θ = 0°, and it decreased $W_{min} = 1.17a + 0.71b$ at θ = 45°. From the information of a = 12.5 μm and b = 27.5 μm, the ultimate interfacing resolution was calculated to be 12.5 μm, and the practical resolution of the S-ACF was 40.8 μm at θ = 45° and 52.5 μm at θ = 0°. Therefore, the S-ACF assured a practical interfacing resolution of 52.5 μm regardless of the alignment. Figure 2E shows the interface by the S-ACF that electrically connects the bottom Au lines to the top Au lines. The line width of the Au line was 100 μm, which was twice larger than the practical resolution of the S-ACF. The top Au lines (A1-E1) were facing the corresponding bottom Au lines (A2-E2). The current-voltage (*I-V*) curves in Fig. 2F indicate that the Au lines facing each other (A1-A2 and B1-B2) were electrically connected as like a continuous line (Al-Al), whereas the Au lines facing aside by 100-μm spacing (A1-B2) were electrically insulating. In the connected lines, the current reached a compliance level (1 mA) of the equipment that was set to prevent an overcurrent in the measurement. In addition, low contact resistance allowed the S-ACF to transmit ac electrical signal in high-frequency range. Coplanar waveguide structure was designed using a PCB to extract the transmission performance of the S-ACF (*56*, *57*). The cutoff frequency of the S-ACF was about 18.5 GHz. The stable performance up to the high frequency is attributed to the low dielectric constant of SEBS-g-MA (ε_r = 2.4) (*58*) and the low mutual inductance between the distant MPs (*59*, *60*). This high operating frequency satisfies the demands on extended frequency bands in high-frequency communication systems (*61*). The details of the measurement and the related data are provided in the Supplementary Materials (Supplementary Text and fig. S8).

Deformable interconnection enabled by chemical bonds

Because the S-ACF aims to interface stretchable circuits to other circuits (rigid, flexible, or stretchable), strong adhesion between the two circuits is essential to prevent delamination and fracture at the interface (fig. S9). The conventional ACF using the metal/epoxy composites requires a high processing temperature (~180°C), which is too high because thermal expansion of the stretchable substrate causes fatal damage in stretchable device components. To increase the interfacial fracture energy and decrease the temperature of the interfacing processing, we introduced functional groups in the substrate surface to create chemical bonds with SEBS-g-MA (Fig. 3A). We modified the polyimide (PI) surfaces with (3-mercaptopropyl) trimethoxysilane (MPTMS) for thiol, 3-aminopropyltriethoxysilane (APTES) for amine, and oxygen plasma for hydroxyl groups (fig. S10). MA groups could react chemically and form covalent bonds with amine, thiol, and hydroxyl groups (Fig. 3B). The reactions are well known from various previous studies (*62*–*66*). The reaction process between SEBS-MA and the amine group of APTES, which is the ring-opening amide reaction, is illustrated in Fig. 3C. Figure 3D exhibits the adhesion force of the bonded interface measured by the T-peel test as shown. A 13-μm-thick SEBS-g-MA thin film was sandwiched between the two surface-treated PI substrates. The chemical bonds were formed at a relatively low temperature (80°C) for 10 min under external pressure of 0.1 MPa (see the video for the bonding process; movie S1). The external pressure for the bonding was applied only for making conformal contact between two layers. The pressure is comparable to the contemporary use in commercial products (table S4). The MA-NH_2 pair had the largest adhesion force; thus, we used the reaction pair afterward. The Fourier transform infrared spectroscopy (FT-IR) results verifying the formation of the chemical bonds are provided in fig. S11. Shear test was conducted using the method of hanging weights on the prepared sample (movie S2). The interface could endure more than 19.6 N (2 kgf).

Electrical stability of the S-ACF interconnection

Figure 4 exhibits the electrical stability of the S-ACF interface between the top and bottom circuit lines (200 μm in width). The flexible lines were Au evaporated on the PI substrate, and the stretchable lines were Ga-In alloy (EGaIn) printed in the PDMS substrate (fig. S12). Detailed methods of fabricating EGaIn circuits are described in Materials and Methods. We used the MA-NH_2 amide bond at S-ACF/PI interface and the Si-O-Si siloxane bond at the S-ACF/PDMS interface. Figure 4A shows the relative current (red line) between a flexible-flexible circuit pair. The interface showed a negligible current change during repeated pressing cycles in the range of 10 to 40 kPa. The interface was more stable in a flexible-stretchable circuit pair (Fig. 4B) and a stretchable-stretchable circuit pair (Fig. 3C). Digital images of the bonded pairs are provided in fig. S13. The current showed no change when the PDMS was stretched repeatedly up to ε = 20%. It is notable that further elongation caused tearing of the PDMS because most of the stress was concentrated at the PDMS interface. In the stretchable-stretchable circuit pair, there was no current variation up to ε = 80% (Fig. 3C). The stability was maintained under repeated stretching cycles at ε = 15% for the stretchable-flexible interface and ε = 50% for the stretchable-stretchable interface (Fig. 3D).

LED demonstration using MP-patterned S-ACF

For economical interfacing, it is desirable to pattern the S-ACF by placing the MPs only at the electrical interfacing area. We rubbed the MP powder on the SEBA-g-MA template, which was patterned by a photomask. Figure 5A exhibits the MP-patterned S-ACF, which was bonded to Au comb pattern electrode on the PI substrate. The MP patterns were formed between two Au circuit lines. We directly integrated μ-LEDs on the MP-patterned region (Fig. 5B). It is noteworthy that the bottom surface of the μ-LEDs was also treated by APTES (fig. S14). As seen in the scheme of the integrated LEDs (Fig. 5C), we used the MP pattern (0.8 mm × 0.4 mm) smaller than the size of the μ-LEDs (1.0 mm × 0.6 mm) to enhance the adhesion by using the contact between the μ-LED and the bare SEBS-g-MA

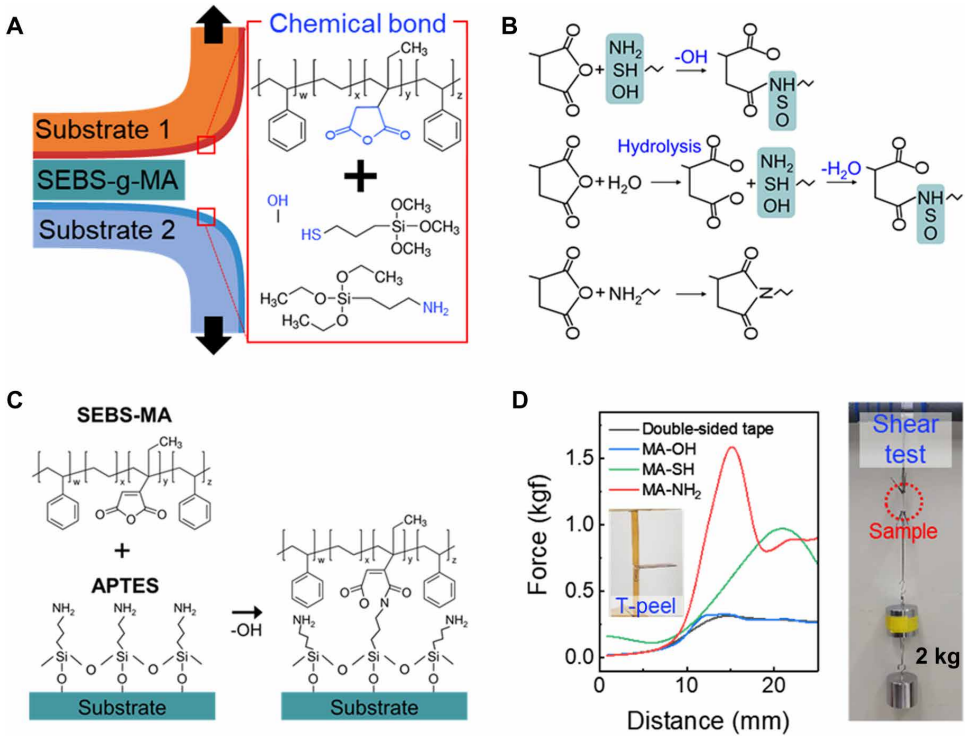

Fig. 3. Chemical treatment results to enhance physical stability of the interface. (**A**) Surface functional groups in the substrates and the scheme of the T-peel adhesion test in the presence of the S-ACF. (**B**) Representative reaction formula between MA and functional groups (amine, thiol, and hydroxyl). (**C**) Scheme of amide bond formation by ring opening of amide reaction between MA in SEBS-g-MA and amine in APTES. (**D**) Adhesion force measured by the peel-off test and the shear test. The inset digital image in the peel-off test shows the real measurement setup of T-peel test. The size of S-ACF for the test was 10 mm × 5 mm. Photo credit: Doowon Park, Department of Materials Science and Engineering, Pohang University of Science and Technology.

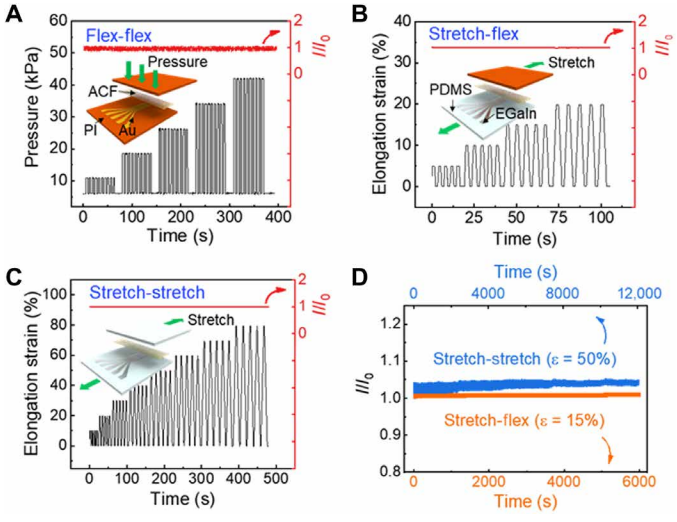

Fig. 4. Electrical performance data indicating high stability under pressure and strain. Relative current changes (I/I_0) of a pair of circuit lines interfaced with the S-ACF during repeated mechanical stimulation. The flexible circuit lines and the stretchable circuit lines were Au/PI and EGaIn/PDMS, respectively. (**A**) Normal pressing on a flex-flex circuit line pair. (**B**) Uniaxial stretching on a stretch-flex circuit line pair. (**C**) Uniaxial stretching on a stretch-stretch circuit line pair. (**D**) Relative current changes in the stretch-stretch and stretch-flex circuit pairs while being stretched over 2000 repeated stretching cycles.

without the MPs (fig. S15). We picked up the μ-LED with a sharp tweezer and transferred it under an OM. The μ-LEDs were bonded by MA-NH_2 amide bond giving heat and pressure (80°C, >0.1 MPa). The patterned S-ACF is expected to be used for vertical interconnections in multilayered devices. The μ-LEDs showed stable performance under repeated bending (Fig. 5D). The μ-LEDs were also integrated, bridging two stretchable circuit lines in the comb-type electrodes (EGaIn/PDMS) (Fig. 5, E and F). The μ-LEDs were operated stably under repeated stretching cycles at a large biaxial elongational strain (areal strain ε_{xy} = 70%; see movie S3). The positions of the MPs deviated slightly from the initial relative alignment at large strains (Fig. 1, D and F); however, the original alignment was reversibly restored at small strains. In practical uses, the S-ACF was strongly adhered to the circuits so that the MPs act like one body with the electronic device. Therefore, the deviation of the MPs is limited, and they can maintain the stable interfacing performance regardless of the degree of the deviation.

DISCUSSION

We designed an S-ACF that assured stable interfacing between stretchable circuit lines and other electrodes (rigid, flexible, or stretchable). The conductive MPs embedded periodically in a thermoplastic block copolymer matrix enabled high-resolution interfacing (1200 μm^2 and 52.5 μm) with a low contact resistance (0.2 ohm per 0.25 mm^2). The use of SEBS-g-MA and the modification of the

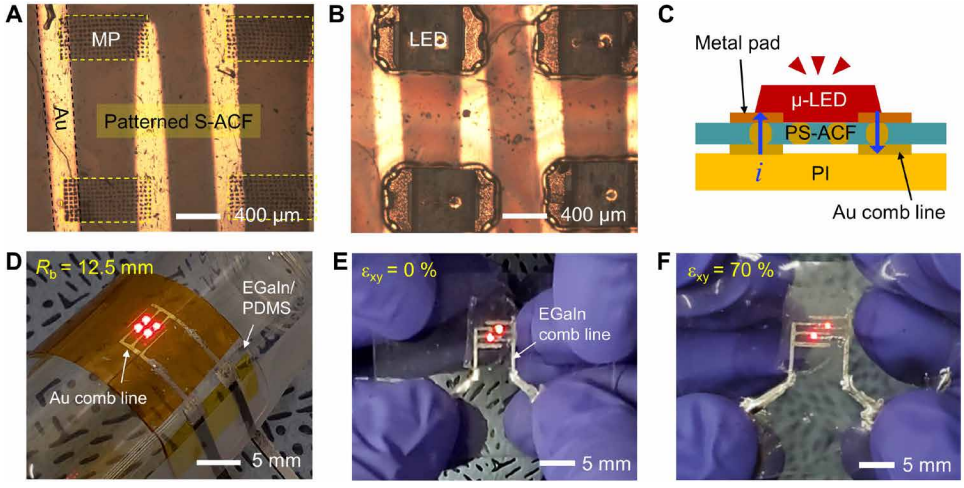

Fig. 5. μ-LED operation with MP-patterned S-ACF on deformable conductive lines. (**A**) OM image of the MP-patterned S-ACF bonded to the flexible comb-structured circuit lines. (**B**) OM image showing the μ-LEDs integrated on the MP-patterned S-ACF. (**C**) Cross-sectional scheme for the μ-LED integration on the interconnected stretchable-flexible circuit lines. (**D**) Digital image of 2 × 2 μ-LEDs on the flexible circuit lines. (**E** and **F**) Digital image of μ-LEDs on the stretchable circuit lines before (E) and after (F) biaxial stretching (ε_{xy} = 70%). Photo credit: Hyejin Hwang; Minsik Kong, Department of Materials Science and Engineering, Pohang University of Science and Technology.

substrate surfaces with amine and hydroxyl groups were made possible to make strong interface only by mild thermal annealing at 80°C for 10 min. The S-ACF exhibited stable electrical performance under high pressure (~40 kPa) and large elongational stretching (ε = 80%). The selectively patterned S-ACF in the size of μ-LEDs opened the possibility of integrating microchips in an economical way. The MP-based S-ACF is advantageous over the via-hole approach in the aspects that SEBS-g-MA between the conductive MPs led to strong adhesion (fig. S15) to the circuit because the polymer surface around the MPs can stabilize the contact between the MP and the metal electrode. In addition, the interfacing is simple without requesting the aligning process that is necessary in the via-hole interface.

This work is the first demonstration of S-ACF, showing the excellent performance in various required properties of ACF, including the biaxial areal stretchability (ε_{xy} = 70%), bonding temperature (80°C), bonding pressure (0.1 MPa), production scalability (>10 cm), and minimum connection area (1200 μm^2) (Fig. 6 and table S4). Although the interconnection with a high spatial resolution has been suggested in a few literatures (*38*, *40*, *47*, *67*), the studies were ACFs for the use in flexible devices. To our best knowledge, high-resolution S-ACF for the use in stretchable devices has not been reported. The S-ACF is expected to be immediately applied to high-density integration of chips, which is a big challenge in stretchable electronics.

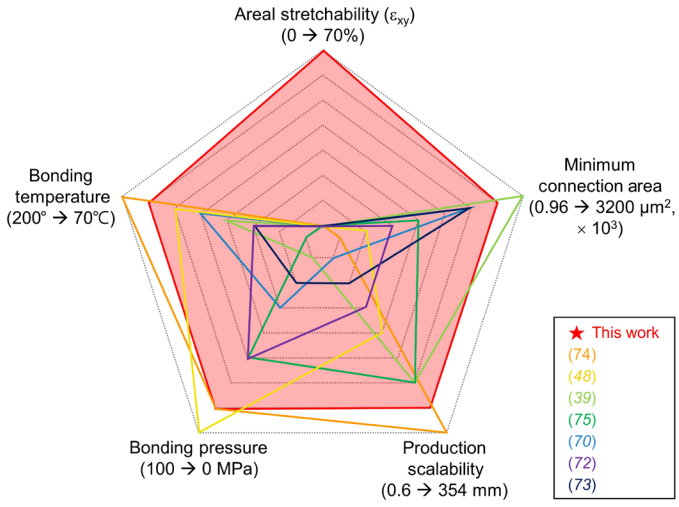

Fig. 6. Spiderweb chart related with the S-ACF. The S-ACFs were ranked for various properties required to ACF (areal stretchability, bonding temperature, bonding pressure, production scalability, and minimum connection area). The numbers in each property indicate the state-of-the-art achievements (the left number is the center in the web chart). The color of the references in the legend matches with the color of the lines in the web.

MATERIALS AND METHODS

Materials

SU-8 50 was purchased from Microchem (USA). A prepolymer of PDMS and the cross-linking agent (Sylgard 184) were purchased from Dow Corning (USA). NOA 61 was purchased from Norland Products Inc. (USA). SEBS-g-MA [MA content ratio of ~2 weight % (wt %)], OTS [weight-average molecular weight (M_w) of ~387.93 g/mol], and polyacrylic acid (PAA) (M_w of ~1800) were purchased from Sigma-Aldrich. Chloroform (99.50%), toluene (99.8%), isopropyl alcohol (IPA), and ethanol (EtOH) were purchased from Samchun Chemicals (Korea). Deionized water was obtained with an 18.2 MΩ system (Vivagen EXL3). The Au-coated conductive MPs (20 μm) were purchased from Duksan Co. (Korea). The PI film of 50 μm thickness was used in this study. The RO4350B substrate of 10-mil thickness for ac transmission test was purchased from Rogers Corporation (USA) and processed by Duri Electronics Co. Ltd. (Korea). Coaxial connectors (2.92 mm) were purchased from Withwave (Korea). For surface modification, MPTMS (95%), APTES (99%), and (3-glycidyloxypropyl)trimethoxysilane (98%) were purchased from Sigma-Aldrich. Chip LEDs (1.0 mm × 0.6 mm, t = 0.2 mm) were purchased from Rohm Semiconductor, Japan.

Fabrication of SU-8 mold

Native Si wafer was cut into 2.5 cm × 2.5 cm after washing and evaporation. SU-8 50 photoresist was spin-coated (500 rpm for 10 s and then 2000 rpm for 30 s) on the cleaned Si wafer. It was prebaked following two steps: 65°C for 10 min and 95°C for 20 min. A photomask was placed on it and exposed by UV light (λ = 365 nm) to 30 mW cm^{-2} for 36 s. Post-baking was performed to the slightly cross-linked photoresist (65°C for 9 min and 95°C for 12 min). Last, the nonexposed SU-8 was dissolved by dipping it in the developer solution for 10 min. The solution was evaporated at 80°C, after rinsing it with IPA. Then, the micropillar-patterned SU-8 structure was obtained.

Fabrication of NOA 61 stamp

The prepared SU-8 pillar structure was used as a mold for soft lithography to fabricate PDMS well pattern. PDMS liquid (10:1 weight ratio of the prepolymer and cross-linker) was poured onto the SU-8 mold and then cured for 3 hours at 80°C. Last, NOA 61 was poured onto the cross-linked PDMS well pattern to obtain the reproducible stamp with proper modulus. It was necessary to degas in NOA 61 liquid to fill into narrow and depth well. The uncured NOA 61 in the PDMS pattern was exposed by UV (131.5 mW cm^{-2} for 20 min) and washed with toluene after it was peeled off from the PDMS. OTS solution (2 wt %) in toluene was spin-coated onto O_2 plasma-treated NOA 61 stamp and slide glass for a carrier substrate.

Fabrication of S-ACF

SEBS-g-MA solution (6, 8, 12, and 16 wt %) in chloroform was spin-coated on PDMS film, and then the solvent was evaporated at 80°C for 10 min. The thickness of the SEBS-g-MA film was mainly governed by the concentration of the polymer solution (fig. S16). To get a uniform thickness, we applied a high spin speed (3000 rpm) for 60 s. The spin condition did not make a difference in the film thickness. The SEBS-g-MA film was placed on OTS-treated slide glass and hot-pressed after covering with the prepared OTS-treated NOA 61 stamp (vacuum state, 180°C, 10 min, 7 MPa). Au/Ni/PS MPs (20 μm in diameter) were rubbed with small piece of PDMS (10:1) on the prepared SEBS-g-MA well pattern. Last, post-hot press was performed to the MP-arrayed SEBS-g-MA film, sandwiched by top and bottom PDMS on slide glass (vacuum state, 235°C, 1 hour, 57 MPa). Then, S-ACF with permanently deformed MPs by compression was obtained.

Stress-strain curve for S-ACF

For sample preparation, S-ACF was cut into 5 mm × 30 mm and then both ends were fixed to a stretcher by a PI adhesive tape. Stress-strain curve was obtained by a stretcher (T95-PE, Linkam Scientific Instruments Ltd., UK) with the following conditions: The stretched S-ACF was about 13 μm in thickness, 5 mm in width, and 5 mm in length. The stretching speed was 50 μm/s. Initial distance was 5 mm.

Stress-strain curve for integrated S-ACF with stretchable and flexible substrates

Both sides of S-ACF were treated by O_2 plasma and then inserted between PDMS and PI film. Hot press was performed at vacuum state, 230°C for 1 hour under 57 MPa. Both ends of the integrated sample were fixed with a gripper and then stretched by the following conditions: The stretched S-ACF was about 250 μm in thickness and 10 mm in width. The stretching speed was 50 μm/s. Initial distance was 16 mm.

Interconnection resistance measurement of S-ACF

For the four-point probe measurement method, Au lines with 0.5 mm in width and 60 nm in thickness were deposited through poly(ethylene terephthalate) shadow mask on the MPTMS-treated PI film. The detailed shape of gold line was proposed in the Supplementary Materials (fig. S6). Thermal evaporator was used for deposition of the Au lines (Teraleader Co. Ltd., Korea). The measurement was performed by applying the constant current of 1 mA to first and second gold lines and measuring the voltage between third and fourth gold lines (Keithley 2450, USA). Interconnection resistance was obtained by converting the measured voltage.

SAM treatment using MPTMS and APTES

PI was cleaned using acetone, IPA, and deionized (DI) water. O_2 plasma (100 W power for 60 s). A total of 200 μl of chemicals was dropped at a petri dish and treated by vapor deposition inside the vacuum chamber for 2 hours. Vapor-treated samples were washed with IPA and DI water to remove remaining chemicals. Hydrolysis and condensation of MPTMS treated over gold were performed by immersing it in dilute hydrochloric acid (3 wt %) for 1 hour and rinsing it with DI water. The self-assembled monolayer (SAM)-treated substrate was finally annealed at the hot plate (100°C) for an additional hour.

Contact angle measurement

PI and chip were surface-treated with the same method as mentioned above. Contact angle was measured using a contact angle meter (Smartdrop Plus, femtobiomed). The same amount of water droplet was carefully dropped by the machine at the same height and measured immediately.

Electrical resolution of integrated S-ACF and circuits

Flexible circuits with 100 μm of five gold lines and 60 nm in thickness were prepared by thermal evaporation through strainless steel shadow mask on the MPTMS-treated PI film. Optimized S-ACF was inserted between two flexible circuits (A1~E1 and A2~E2), and then thermal compression was performed on (Au/PI)/S-ACF/(Au/PI). The *I-V* curves were obtained with a probe station (model 8000, MS Tech, Korea) and a parameter analyzer (4200A-SCS, Keithley, USA). The compliance level was 1 mA.

T-peel test

Peel-off test samples were fabricated by hot pressing [pressure (57 MPa) and temperature (80°C)] the sample film between two surface-treated PI films (width, 1 cm) for 10 min. The surface treatment method on PI was the same as mentioned above. Peel strength was measured using a tensile test machine (DB35-10, Bongshin). The tensile testing speed was 5 mm/min.

Stretchable circuit using EGaIn

For the lines less than 200-μm line width, the EGaIn lines were fabricated by following the previous method (*68*). We thermally evaporated Cr (20 nm)/Cu (100 nm) through a patterned metal mask on the PDMS substrate and used it as an adhesive metal layer. EGaIn was bar-coated over the metal Cr/Cu lines inside a NaOH solution bath (5 wt %). EGaIn was positioned only on the metal lines due to the poor wettability to PDMS but the good wettability to the Cr/Cu.

For the lines larger than 200-μm line width, an aqueous PAA solution (5 wt %) was spin-coated (1000 rpm, 60 s) on a glass slide. EGaIn was patterned directly on the PAA layer through a metal mask, and brushing was applied to remove EGaIn on the metal mask. PDMS (10:1) was spin-coated (500 rpm, 30 s) on the EGaIn-coated PAA layer and stored at an oven (80°C) for 3 hours for cross-linking. The entire sample was immersed in DI water for 12 hours to remove and dissolve the PAA layer. Detaching the PDMS from the glass slide produced the EGaIn lines.

Deformability test of S-ACF

For interconnection of flexible-flexible circuits, APTES-treated Au lines (200 μm in width) on the PI film were prepared. Amine from the PI film and MA of S-ACF were bonded by facing the interfaces at 80°C and a slight touch (>0.1 MPa). Normal pressure from 10 to 40 kPa was applied onto the bonded region by UMP 100 (Teraleader Co. Ltd., Korea). For the stretchable-flexible circuits, the MA-NH_2 amide bond was induced at the S-ACF/PI interfaces and the siloxane bond at the S-ACF/PDMS interface at the same bonding conditions (80°C, 0.1 MPa). It is notable that the PDMS was oxygen plasma–treated to create the silanol groups before the bonding process. Rigid μ-LEDs were integrated on a patterned S-ACF with the same bonding process. The integrated samples [stretchable-flexible, stretchable-stretchable, and stretchable (flexible)–rigid interconnection] were elongated by UMP 100. In all measurements, the change in current was obtained at the applied voltage of 1 V (Keithley 2400, USA).

SUPPLEMENTARY MATERIALS

Supplementary material for this article is available at http://advances.sciencemag.org/cgi/content/full/7/32/eabh0171/DC1

REFERENCES AND NOTES

1. Y. Hwang, J. H. Lee, Y. H. Kim, S. Jeong, S. Y. Lee, J. Jung, J. H. Kim, Y. Choi, S. Jung, Lubricant-added conductive composite for direct writing of a stretchable electrode. *ACS Appl. Mater. Interfaces* **11**, 48459–48465 (2019).
2. T. Sekitani, H. Nakajima, H. Maeda, T. Fukushima, T. Aida, K. Hata, T. Someya, Stretchable active-matrix organic light-emitting diode display using printable elastic conductors. *Nat. Mater.* **8**, 494–499 (2009).
3. J. Liang, L. Li, X. Niu, Z. Yu, Q. Pei, Elastomeric polymer light-emitting devices and displays. *Nat. Photonics* **7**, 817–824 (2013).
4. C. Larson, B. Peele, S. Li, S. Robinson, M. Totaro, L. Beccai, B. Mazzolai, R. Shepherd, Highly stretchable electroluminescent skin for optical signaling and tactile sensing. *Science* **351**, 1071–1074 (2016).
5. M. Amjadi, K.-U. Kyung, I. Park, M. Sitti, Stretchable, skin-mountable, and wearable strain sensors and their potential applications: A review. *Adv. Funct. Mater.* **26**, 1678–1698 (2016).
6. Y. Yamada, T. Morizono, Y. Umetani, H. Takahashi, Highly soft viscoelastic robot skin with a contact object-location-sensing capability. *IEEE Trans. Ind. Electron.* **52**, 960–968 (2005).
7. H. U. Chung, A. Y. Rwei, A. Hourlier-Fargette, S. Xu, K. Lee, E. C. Dunne, Z. Xie, C. Liu, A. Carlini, D. H. Kim, D. Ryu, E. Kulikova, J. Cao, I. C. Odland, K. B. Fields, B. Hopkins, A. Banks, C. Ogle, D. Grande, J. B. Park, J. Kim, M. Irie, H. Jang, J. Lee, Y. Park, J. Kim, H. H. Jo, H. Hahm, R. Avila, Y. Xu, M. Namkoong, J. W. Kwak, E. Suen, M. A. Paulus, R. J. Kim, B. V. Parsons, K. A. Human, S. S. Kim, M. Patel, W. Reuther, H. S. Kim, S. H. Lee, J. D. Leedle, Y. Yun, S. Rigali, T. Son, I. Jung, H. Arafa, V. R. Soundararajan, A. Ollech, A. Shukla, A. Bradley, M. Schau, C. M. Rand, L. E. Marsillio, Z. L. Harris, Y. Huang, A. Hamvas, A. S. Paller, D. E. Weese-Mayer, J. Y. Lee, J. A. Rogers, Skin-interfaced biosensors for advanced wireless physiological monitoring in neonatal and pediatric intensive-care units. *Nat. Med.* **26**, 418–429 (2020).
8. G. Chen, N. Matsuhisa, Z. Liu, D. Qi, P. Cai, Y. Jiang, C. Wan, Y. Cui, W. R. Leow, Z. Liu, S. Gong, K.-Q. Zhang, Y. Cheng, X. Chen, Plasticizing silk protein for on-skin stretchable electrodes. *Adv. Mater.* **30**, 1800129 (2018).
9. T. Kim, J. Park, J. Sohn, D. Cho, S. Jeon, Bioinspired, highly stretchable, and conductive dry adhesives based on 1D–2D hybrid carbon nanocomposites for all-in-one ECG electrodes. *ACS Nano* **10**, 4770–4778 (2016).
10. S. Baik, D. W. Kim, Y. Park, T.-J. Lee, S. H. Bhang, C. Pang, A wet-tolerant adhesive patch inspired by protuberances in suction cups of octopi. *Nature* **546**, 396–400 (2017).
11. A. Miyamoto, S. Lee, N. F. Cooray, S. Lee, M. Mori, N. Matsuhisa, H. Jin, L. Yoda, T. Yokota, A. Itoh, M. Sekino, H. Kawasaki, T. Ebihara, M. Amagai, T. Someya, Inflammation-free, gas-permeable, lightweight, stretchable on-skin electronics with nanomeshes. *Nat. Nanotechnol.* **12**, 907–913 (2017).
12. W. Zhou, S. Yao, H. Wang, Q. Du, Y. Ma, Y. Zhu, Gas-permeable, ultrathin, stretchable epidermal electronics with porous electrodes. *ACS Nano* **14**, 5798–5805 (2020).
13. H. W. Kim, T. Y. Kim, H. K. Park, I. You, J. Kwak, J. C. Kim, H. Hwang, H. S. Kim, U. Jeong, Hygroscopic auxetic on-skin sensors for easy-to-handle repeated daily use. *ACS Appl. Mater. Interfaces* **10**, 40141–40148 (2018).
14. I. You, D. G. Mackanic, N. Matsuhisa, J. Kang, J. Kwon, L. Beker, J. Mun, W. Suh, T. Y. Kim, J. B.-H. Tok, Z. Bao, U. Jeong, Artificial multimodal receptors based on ion relaxation dynamics. *Science* **370**, 961–965 (2020).
15. J. Park, J. Kim, S.-Y. Kim, W. H. Cheong, J. Jang, Y.-G. Park, K. Na, Y.-T. Kim, J. H. Heo, C. Y. Lee, J. H. Lee, F. Bien, J.-U. Park, Soft, smart contact lenses with integrations of wireless circuits, glucose sensors, and displays. *Sci. Adv.* **4**, eaap9841 (2018).
16. S. I. Park, D. S. Brenner, G. Shin, C. D. Morgan, B. A. Copits, H. U. Chung, M. Y. Pullen, K. N. Noh, S. Davidson, S. J. Oh, J. Yoon, K.-I. Jang, V. K. Samineni, M. Norman, J. G. Grajales-Reyes, S. K. Vogt, S. S. Sundaram, K. M. Wilson, J. S. Ha, R. Xu, T. Pan, T.-I. Kim, Y. Huang, M. C. Montana, J. P. Golden, M. R. Bruchas, R. W. Gereau IV, J. A. Rogers, Soft, stretchable, fully implantable miniaturized optoelectronic systems for wireless optogenetics. *Nat. Biotechnol.* **33**, 1280–1286 (2015).
17. D.-H. Kim, J. Viventi, J. J. Amsden, J. Xiao, L. Vigeland, Y.-S. Kim, J. A. Blanco, B. Panilaitis, E. S. Frechette, D. Contreras, D. L. Kaplan, F. G. Omenetto, Y. Huang, K.-C. Hwang, M. R. Zakin, B. Litt, J. A. Rogers, Dissolvable films of silk fibroin for ultrathin conformal bio-integrated electronics. *Nat. Mater.* **9**, 511–517 (2010).
18. Y. Liu, J. Liu, S. Chen, T. Lei, Y. Kim, S. Niu, H. Wang, X. Wang, A. M. Foudeh, J. B.-H. Tok, Z. Bao, Soft and elastic hydrogel-based microelectronics for localized low-voltage neuromodulation. *Nat. Biomed. Eng.* **3**, 58–68 (2019).
19. Y.-G. Park, H. S. An, J.-Y. Kim, J.-U. Park, High-resolution, reconfigurable printing of liquid metals with three-dimensional structures. *Sci. Adv.* **5**, eaaw2844 (2019).
20. M.-G. Kim, D. K. Brown, O. Brand, Nanofabrication for all-soft and high-density electronic devices based on liquid metal. *Nat. Commun.* **11**, 1002 (2020).
21. W.-J. Song, M. Kong, S. Cho, S. Lee, J. Kwon, H. B. Son, J. H. Song, D.-G. Lee, G. Song, S.-Y. Lee, S. Jung, S. Park, U. Jeong, Stand-alone intrinsically stretchable electronic device platform powered by stretchable rechargeable battery. *Adv. Funct. Mater.* **30**, 2003608 (2020).
22. K. Toyozawa, K. Fujita, S. Minamide, T. Maeda, Development of copper wire bonding application technology. *IEEE Trans. Components Hybrids Manuf. Technol.* **13**, 667–672 (1990).
23. Z. W. Zhong, Overview of wire bonding using copper wire or insulated wire. *Microelectron. Reliab.* **51**, 4–12 (2011).
24. T. Kawase, H. Sirringhaus, R. H. Friend, T. Shimoda, Inkjet printed via-hole interconnections and resistors for all-polymer transistor circuits. *Adv. Mater.* **13**, 1601–1605 (2001).
25. E. Laermans, J. D. Geest, D. De Zutter, F. Olyslager, S. Sercu, D. Morlion, Modeling complex via hole structures. *IEEE Trans. Adv. Packag.* **25**, 206–214 (2002).
26. A. Singh, D. A. Horsley, M. B. Cohn, A. P. Pisano, R. T. Howe, Batch transfer of microstructures using flip-chip solder bonding. *J. Microelectromech. Syst.* **8**, 27–33 (1999).
27. S. Tanaka, S.-H. Jeong, S. Sekiguchi, T. Kurahashi, Y. Tanaka, K. Morito, High-output-power, single-wavelength silicon hybrid laser using precise flip-chip bonding technology. *Opt. Express* **20**, 28057–28069 (2012).
28. Y. Sun, W. M. Choi, H. Jiang, Y. Y. Huang, J. A. Rogers, Controlled buckling of semiconductor nanoribbons for stretchable electronics. *Nat. Nanotechnol.* **1**, 201–207 (2006).
29. Z. Liu, P. S. Valvo, Y. Huang, Z. Yin, Cohesive failure analysis of an array of IC chips bonded to a stretched substrate. *Int. J. Solids Struct.* **50**, 3528–3538 (2013).
30. J.-Y. Sun, N. Lu, J. Yoon, K.-H. Oh, Z. Suo, J. J. Vlassak, Debonding and fracture of ceramic islands on polymer substrates. *J. Appl. Phys.* **111**, 013517 (2012).
31. N. Lu, J. Yoon, Z. Suo, Delamination of stiff islands patterned on stretchable substrates. *Int. J. Mater. Res.* **98**, 717–722 (2007).
32. T. Ye, Z. Suo, A. G. Evans, Thin film cracking and the roles of substrate and interface. *Int. J. Solids Struct.* **29**, 2639–2648 (1992).
33. D. G. Marques, P. A. Lopes, A. T. de Almeida, C. Majidi, M. Tavakoli, Reliable interfaces for EGaIn multi-layer stretchable circuits and microelectronics. *Lab Chip* **19**, 897–906 (2019).
34. S. Lee, S. Gandla, M. Naqi, U. Jung, H. Youn, D. Pyun, Y. Rhee, S. Kang, H.-J. Kwon, H. Kim, M. G. Lee, S. Kim, All-day mobile healthcare monitoring system based on heterogeneous stretchable sensors for medical emergency. *IEEE Trans. Ind. Electron.* **67**, 8808–8816 (2020).
35. Y.-S. Kim, J. Lu, B. Shih, A. Gharibans, Z. Zou, K. Matsuno, R. Aguilera, Y. Han, A. Meek, J. Xiao, M. T. Tolley, T. P. Coleman, Scalable manufacturing of solderable and stretchable physiologic sensing systems. *Adv. Mater.* **29**, 1701312 (2017).

36. Y. Ko, J. Oh, K. T. Park, S. Kim, W. Huh, B. J. Sung, J. A. Lim, S.-S. Lee, H. Kim, Stretchable conductive adhesives with superior electrical stability as printable interconnects in washable textile electronics. *ACS Appl. Mater. Interfaces* **11**, 37043–37050 (2019).
37. Z. Lai, J. Liu, Anisotropically conductive adhesive flip-chip bonding on rigid and flexible printed circuit substrates. *IEEE Trans. Compon. Packag. Manuf. Technol.* **19**, 644–660 (1996).
38. J.-H. Park, J. C. Park, S. Lee, K.-W. Paik, Piezoelectric ceramics and flexible printed circuits' interconnection using Sn58Bi solder anisotropic conductive films for flexible ultrasound transducer assembly. *IEEE Trans. Compon. Packag. Manuf. Technol.* **9**, 1897–1903 (2019).
39. J.-H. Byeon, D.-J. Yoon, K.-W. Paik, A study on the magnetic dispersion of the conductive particles of anchoring-polymer-layer anisotropic conductive films and its fine-pitch interconnection properties. *IEEE Trans. Compon. Packag. Manuf. Technol.* **9**, 1235–1243 (2019).
40. J. S. Lee, S. J. Kang, J. H. Shin, Y. J. Shin, B. Lee, J.-M. Koo, T.-i. Kim, Nanoscale-dewetting-based direct interconnection of microelectronics for a deterministic assembly of transfer printing. *Adv. Mater.* **32**, 1908422 (2020).
41. Z. Xue, H. Song, J. A. Rogers, Y. Zhang, Y. Huang, Mechanically-guided structural designs in stretchable inorganic electronics. *Adv. Mater.* **32**, 1902254 (2020).
42. G.-T. Park, S. J. Lee, B. G. Kim, High thermally conductive epoxy composite inks cured by infrared laser irradiation for two-dimensional/three-dimensional printing technology. *J. Compos. Mater.* **54**, 4635–4643 (2020).
43. L. Mo, Z. Guo, L. Yang, Q. Zhang, Y. Fang, Z. Xin, Z. Chen, K. Hu, L. Han, L. Li, Silver nanoparticles based ink with moderate sintering in flexible and printed electronics. *Int. J. Mol. Sci.* **20**, 2124 (2019).
44. W. Xu, Y. Wei, Strength and interface failure mechanism of adhesive joints. *Int. J. Adhes. Adhes.* **34**, 80–92 (2012).
45. T. Salo, A. Halme, M. Kanerva, J. Vanhala, Bond strength and failure mechanisms of nonconductive adhesives for stretchable electronics. *IEEE Trans. Compon. Packag. Manuf. Technol.* **10**, 770–778 (2020).
46. R. Atif, F. Inam, Modeling and simulation of graphene based polymer nanocomposites: Advances in the last decade. *Graphene* **5**, 96–142 (2016).
47. T. Lu, J. Wissman, Ruthika, C. Majidi, Soft anisotropic conductors as electric vias for ga-based liquid metal circuits. *ACS Appl. Mater. Interfaces* **7**, 26923–26929 (2015).
48. C. Park, T. Lee, Y. Xia, T. J. Shin, J. Myoung, U. Jeong, Quick, large-area assembly of a single-crystal monolayer of spherical particles by unidirectional rubbing. *Adv. Mater.* **26**, 4633–4638 (2014).
49. C. Park, K. Koh, U. Jeong, Structural color painting by rubbing particle powder. *Sci. Rep.* **5**, 8340 (2015).
50. H. Hwang, Y. Kim, J.-H. Park, U. Jeong, 2D percolation design with conductive microparticles for low-strain detection in a stretchable sensor. *Adv. Funct. Mater.* **30**, 1908514 (2020).
51. K. Koh, H. Hwang, C. Park, J. Y. Lee, T. Y. Jeon, S.-H. Kim, J. K. Kim, U. Jeong, Large-area accurate position registry of microparticles on flexible, stretchable substrates using elastomer templates. *ACS Appl. Mater. Interfaces* **8**, 28149–28158 (2016).
52. H. Hwang, S.-E. Choi, S. W. Han, I. You, E. S. Jeong, S. Kim, H. Yang, S. Lee, J. Choo, J. W. Kim, U. Jeong, Cut-and-Paste transferrable pressure sensing cartridge films. *Chem. Mater.* **30**, 6410–6419 (2018).
53. W. J. Lee, S. W. Han, I. You, S.-E. Choi, U. Jeong, J. W. Kim, Conductive magnetic-patchy colloidal microparticles for a high performance pressure sensor. *Chem. Commun.* **52**, 12334–12337 (2016).
54. I. You, S. E. Choi, H. Hwang, S. W. Han, J. W. Kim, U. Jeong, E-skin tactile sensor matrix pixelated by position-registered conductive microparticles creating pressure-sensitive selectors. *Adv. Funct. Mater.* **28**, 1801858 (2018).
55. S.-E. Choi, D. Park, H. Hwang, M. Seo, D. Lee, U. Jeong, J. W. Kim, 2D colloidal array of glucose-conjugative conductive microparticles for a pressure-mediated chemiresistive sensor platform. *Adv. Funct. Mater.* **30**, 2000431 (2020).
56. M. J. Yim, W. H. Ryu, Y. D. Jeon, J. H. Lee, S. Y. Ahn, J. H. Kim, K. W. Paik, Microwave model of anisotropic conductive film flip-chip interconnection for high frequency applications. *IEEE Trans. Compon. Packag. Technol.* **22**, 575–581 (1999).
57. J. Kim, Y.-C. Lee, S.-S. Ha, J.-M. Koo, J.-H. Ko, W. Nah, S.-B. Jung, Electrical characterization of adhesive flip chip interconnects for microwave application. *J. Micro/Nanolithogr. MEMS MOEMS* **7**, 023007 (2008).
58. E. Helal, N. R. Demarquette, E. David, M. Frechette, paper presented at the 2015 IEEE Conference on Electrical Insulation and Dielectric Phenomena (CEIDP), Ann Arbor, MI, 18 to 21 October 2015.
59. M. J. Yim, I. H. Jeong, H.-K. Choi, J.-S. Hwang, J.-Y. Ahn, W. Kwon, K.-W. Paik, Flip chip interconnection with anisotropic conductive adhesives for RF and high-frequency applications. *IEEE Trans. Compon. Packag. Manuf. Technol.* **28**, 789–796 (2005).
60. M. J. Yim, W. Kwon, K. W. Paik, Effect of filler content on the dielectric properties of anisotropic conductive adhesives materials for high-frequency flip–chip interconnection. *Mater. Sci. Eng. B* **126**, 59–65 (2006).
61. W. Saad, M. Bennis, M. Chen, A Vision of 6G wireless systems: Applications, trends, technologies, and open research problems. *IEEE Netw.* **34**, 134–142 (2019).
62. K. Liu, W. Stadlbauer, G. Zitzenbacher, C. Paulik, C. Burgstaller, Effects of surface modification of talc on mechanical properties of polypropylene/talc composites. *AIP Conf. Proc.* **1713**, 120008 (2016).
63. M. Kour, R. Gupta, R. K. Bansal, Experimental and theoretical investigation of the reaction of secondary amines with maleic anhydride. *Aust. J. Chem.* **70**, 1247 (2017).
64. M. Podgórski, S. Mavila, S. Huang, N. Spurgin, J. Sinha, C. N. Bowman, Thiol–Anhydride dynamic reversible networks. *Angew. Chem. Int. Ed.* **59**, 9345–9349 (2020).
65. V. Leiro, P. Parreira, S. C. Freitas, M. C. L. Martins, A. P. Pêgo, Conjugation chemistry principles and surface functionalization of nanomaterials, in *Biomedical Applications of Functionalized Nanomaterials* (Elsevier, 2018), pp. 35–66.
66. D. A. Echeverri, V. Cádiz, J. C. Ronda, L. A. Rios, Synthesis of elastomeric networks from maleated soybean-oil glycerides by thiol-ene coupling. *Eur. Polym. J.* **48**, 2040–2049 (2012).
67. Dexerials Corporation, PAF 700 series; www.dexerials.jp/en/products/acf/paf700.html.
68. I. D. Joshipura, H. R. Ayers, C. Majidi, M. D. Dickey, Methods to pattern liquid metals. *J. Mater. Chem. C* **3**, 3834–3841 (2015).
69. D. M. Pozar, Rectangular cavity modes, in *Microwave Engineering* (Wiley, ed. 3, 2005), p. 120.
70. Shin-Etsu Polymer Co. Ltd., GB-Matrix type; www.shinpoly.co.jp/en/product/product/electric/gb-matrix.html.
71. Showa Denko Materials (America) Inc., AC-4000 series; www.ma.showadenko.com/products_do_01_1.htm.
72. H&SHighTech Corp., TCF7040/41 series; www.telephus.com/02_01_04.php.
73. 3M, ECATT 9703; multimedia.3m.com/mws/media/66235O/3m-electrically-conductive-adhesive-transfer-tape-9703.pdf.
74. D.-J. Yoon, S.-H. Lee, K.-W. Paik, Effects of polyacrylonitrile anchoring polymer layer solder anisotropic conductive films on the solder ball movement for fine-pitch Flex-on-Flex (FOF) assembly. *IEEE Trans. Compon. Packag. Manuf. Technol.* **9**, 830–835 (2019).

Acknowledgments

Funding: This research was financially supported by the Basic Science Research Program through the National Research Foundation of Korea (NRF) funded by the Ministry of Education (No. 2021M3H4A1A03049084 and 2021M3H4A1A03049084). **Author contributions:** H.H., M.K., and U.J. designed and wrote this work with interdisciplinary analysis from K.K., D.P., S.L., S.P., and H.-J.S. K.K. discussed and measured the electrical conduction properties of the S-ACF. D.P. performed the FT-IR and shear test. S.L. performed the peel-off test. Conceptualization: H.H., M.K., and U.J. Methodology: H.H., M.K., K.K., and U.J. Investigation: H.H., M.K., K.K., S.L., and D.P. Visualization: H.H. and M.K. Supervision: S.P., H.-J.S., and U.J. Writing (original draft): H.H. and M.K. Writing (review and editing): H.H., M.K., and U.J. **Competing interests:** A Korean patent based on the results of this study is filed by Pohang University of Science and Technology (POSTECH) (application number: 10-2020-0172368; application date: 10 December 2020; authors: Hyejin Hwang, Minsik Kong, Unyong Jeong). The authors declare no other competing interests. **Data and materials availability:** All data needed to evaluate the conclusions in the paper are present in the paper and/or the Supplementary Materials.

Submitted 10 February 2021
Accepted 21 June 2021
Published 6 August 2021
10.1126/sciadv.abh0171

Citation: H. Hwang, M. Kong, K. Kim, D. Park, S. Lee, S. Park, H.-J. Song, U. Jeong, Stretchable anisotropic conductive film (S-ACF) for electrical interfacing in high-resolution stretchable circuits. *Sci. Adv.* **7**, eabh0171 (2021).